Please fill in the name of the event you are preparing this manuscript for.	SPE Asia Pacific Oil & Gas Conference and Exhibition
Please fill in your 6-digit SPE manuscript number.	SPE-191962-MS
Please fill in your manuscript title.	Statistical Analysis of Effect of Sensor Degradation and Heat Transfer Modeling on Multiphase Flowrate Estimates from a Virtual Flow Meter

Please fill in your author name(s) and company affiliation.

Given Name	Surname	Company
Timur	Bikmukhametov	Norwegian University of Science and Technology
Milan	Stanko	Norwegian University of Science and Technology
Johannes	Jäschke	Norwegian University of Science and Technology

Abstract

Accurate flowrate measurements in petroleum production systems are important for optimization, fiscal metering, and production allocation. Sometimes, Virtual Flow Meters (VFMs) are used for this purpose instead of physical meters to reduce cost. These systems estimate the flowrates using a computational model that represents accurately the production system of interest. Since VFM systems mostly rely on pressure and temperature measurements, it is important to understand how accuracy and degradation of sensors influence the VFM flowrate estimates.

In this work, a VFM system for a subsea oil well was created using a transient multiphase model built in a commercial software and controlled from an external computational routine. A statistical analysis of VFM simulation results was performed to quantify the effect of sensor degradation on the VFM flowrate estimates. In addition, the effect of temperature matching and a segmented approach to represent the well heat transfer were evaluated.

The analysis showed that the sensor degradation effect should be considered in VFM systems carefully, especially if a high estimation accuracy is required. Measurement drift was found to be the most critical factor of the sensor degradation but high measurement noise can also cause considerable errors of the flowrate estimates. In addition, it was found that a complex representation of the wellbore heat transfer is not required to obtain accurate flowrate predictions and simplified models can be used instead.

Introduction

In oil and gas production, continuous information about oil, gas and water flowrates from each well is important for production optimization, rate allocation and reservoir management (Falcone et al. 2001). In offshore field developments, it is often the case that the field has shared licenses so that accurate estimates of the produced volume of hydrocarbons are essential to determine partner share. This case also holds for smaller subsea fields which are tied-in with the existing infrastructures.

In addition to the conventional approach of flowrate estimation using well test separators, physical multiphase flow meters (MPFM) are used for this purpose (Falcone et al. 2009). The advantage of the multiphase flow meters is the fact that they can measure flowrates without separating the oil, gas and water streams first as it is typically performed in test separators. By mounting them inline on the well template, there is no need to re-route well production to perform the testing, thus, measurements can be often obtained in real-time. On the other hand, these devices are expensive and exposed to failures and degradation which requires costly interventions for repair or replacement of the meters (Patel et al. 2014).

Another alternative is Virtual Flow Metering. This technology uses measurements from sensors (typically pressure and temperature) together with a numerical model of the system to estimate flowrates. Depending on the extension and type of the model, it usually requires some information about physical parameters of the system (e.g. pipe size, fluid properties, thermodynamic behavior and choke opening) as presented by Holmås and Løvli (2011) and Melbø et al. (2003). By combining all this information, it is possible to estimate the flowrates of oil, gas and water by modeling specific parts of the production system such as wellbore, choke, near-well region or using a combination of these models (Haldipur and Metcalf 2008). The discrepancies between the estimated and reference parameters can be minimized using an optimization algorithm (Holmås and Løvli 2011).

Since Virtual Flow Meters rely on sensor readings for real-time flowrate estimation, it is important to understand the influence of the sensors accuracy on the flowrate predictions. In general, sensors in oil and gas wells are exposed to harsh conditions such as high pressure and temperature, sand erosion and scaling. This is particularly true for downhole sensors. Such conditions cause mechanical degradation which increases the measurement noise and drift. (Kikani et al. 1997). As such, one of the questions addressed in this paper is how the sensor degradation impacts the VFM flowrate estimates. A somewhat similar question was addressed by Tangen et al. (2017) and Lansangan (2012). In both cases, the authors introduced an error to the measurements and estimated the VFM accuracy. However, in the analysis only extreme values were considerd, i.e. only the maximum deviations of the flowrates were calculated for specific values of the measurement errors.

In this paper, in addition to the extreme values, we estimate the entire probabilistic distribution of the flowrates and compare the distribution parameters under various measurement errors to estimate the trend. To do this, we performed multiple simulations under random measurement errors and evaluated the results using statistical methods. The results of this analysis can contribute to a deeper understanding by VFM customers about the effect of the measurement error on the flowrate estimates, such that they can evaluate when this effect is important and should be considered during the field operation.

Another aspect which can influence the precision of the flowrate estimates is the fidelity of the applied models. For example, in a VFM system we can assume that the heat transfer coefficient is constant along the wellbore and then use it as a tuning parameter to fit a specific temperature at the wellhead. However, in reality the heat transfer coefficient varies along the wellbore due to the mechanical structure of the well. In this paper, we consider both constant and varying heat transfer coefficients for the heat transfer VFM part to study the difference between the approaches. The results from this study can contribute to optimization of VFM tuning strategies in terms of accuracy and computational time.

Well architecture and fluid properties

In this study, we consider a subsea oil well. The well consists of a conductor, surface, intermediate and production casings, liner and tubing. **Fig. 1** shows the well profile and the mechanical structure, fluid properties and formation parameters. For the heat transfer modeling study, the well is divided into 5 sections based on the number of layers in a particular section. The walls of the tubing pipes with thickness ω_j are shown in black color, cement is represented in grey and mud in yellow. All radial distances from the well center line are shown as R_j.

The model employed in the VFM scheme considers only the flow in the tubing, so that we do not include choke simulations. As such, we utilize the following measurements:

- Bottomhole pressure (P_{wf})
- Bottomhole temperature (T_{wf})
- Wellhead pressure (P_{wh})
- Wellhead temperature (T_{wh})

PVTsim was used to generate fluid properties based on a given composition using Equations-of-State (EOS) approach. The bottomhole temperature is assumed to be equal to the reservoir temperature. The geothermal gradient is linearly interpolated from the reservoir to the seabed conditions.

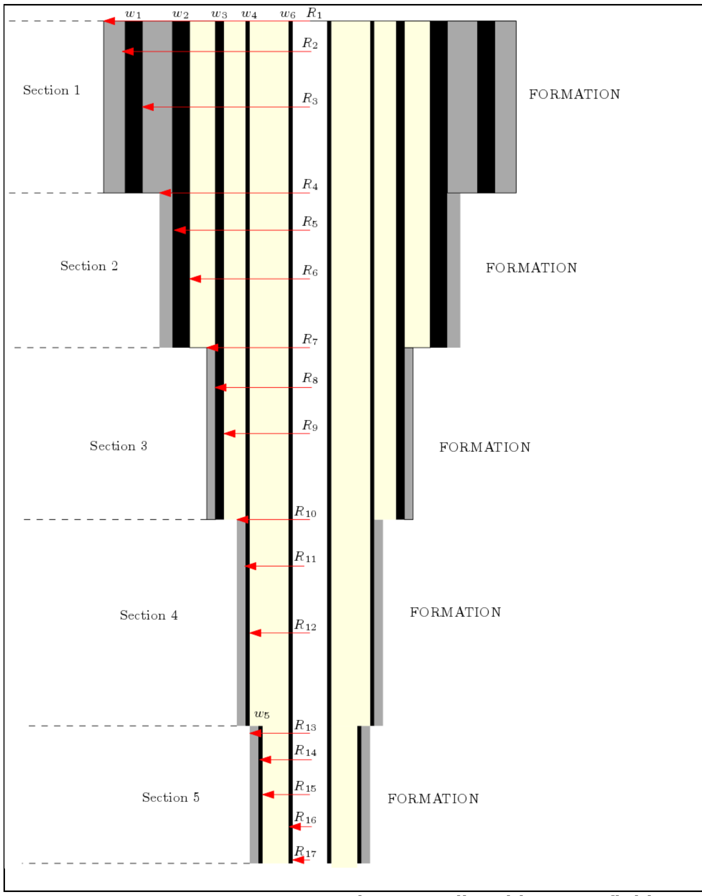

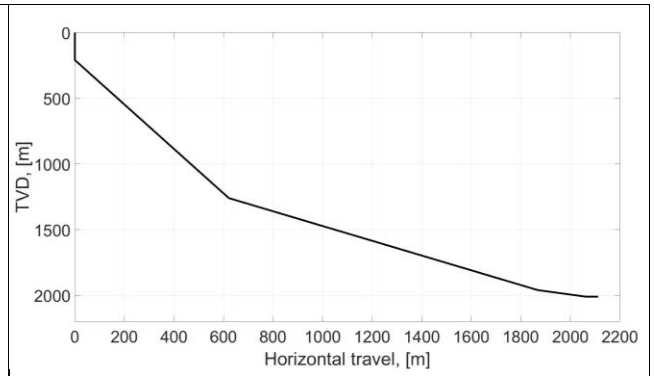

Parameter	Value
GOR, Sm^3/Sm^3	153.7
WC, %	30
Total well length, m	3110
Tubing inner diameter, m	0.0622
Bottomhole pressure, bar	160
Wellhead pressure, bar	40
Bottomhole temperature, ºC	70
Wellhead temperature, ºC	57
Reservoir temperature, ºC	70
Seabed temperature, ºC	8
Formation heat conductivity, W/m.K	1.5912
Wall heat conductivity, W/m.K	45.2573
Cement heat conductivity, W/m.K	0.98
Mud heat conductivity, W/m.K	0.6054
Formation heat diffusivity, m^2/h	0.003716

Fig. 1 – Well architecture, fluid properties and system parameters

VFM system

The VFM system employed consists of two parts: a model of the physical system and an optimization algorithm. The model is built in such a way that some of the parameters that are measured are an output, and the flowrate is an input, thus the optimization solver is employed to obtain the flowrate that minimizes the difference between measured and predicted values. The constructed VFM system is based on commercial packages: OLGA and MATLAB. OLGA is a well-known multiphase flow simulator and has been extensively used in the industry for computing transient multiphase flow. MATLAB is a multifunctional computing environment with its own programming language and various computational toolboxes. To link OLGA and MATLAB, we use Matrikon OPC server. The main goal of this tool is to read signals from one software and transfer it to another one. A schematic representation of the constructed VFM tool is shown in **Fig. 2** on the left.

In OLGA, for given pressures and temperatures we run transient multiphase flow simulations until they reach a steady state. In MATLAB, we use the interior-point numerical optimization algorithm to find a flowrate that minimizes an objective function of the following form:

$$\sum_i \left(\frac{X_{meas\,i} - X_{OLGA\,i}}{\sigma_i} \right)^2 \tag{1}$$

where $X_{meas\,i}$ denotes measured value, $X_{OLGA\,i}$ – the predicted value, σ_i – the measurement uncertainty, i – the measurement index.

The computational procedure is shown in Fig. 2 on the right. To initiate the procedure, we introduce an initial guess in the mass source node. Then, the optimization solver iteratively computes finite difference gradients and adjusts the flowrate until the cost converges to a minimum.

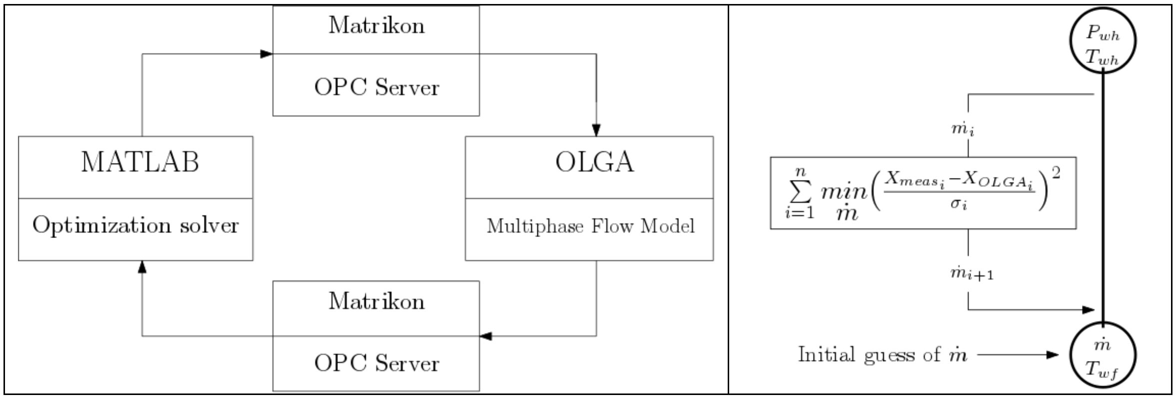

Fig. 2 – Schematic representation of the VFM system (left) and computational procedure (right).
(To start the computational procedure, we introduce an initial guess of the flowrate to OLGA which computes the associated wellhead temperature and bottomhole pressure. Then, these values go to the optimization solver which computes the finite difference gradients and iteratively changes the flowrate value until the minimum of the cost function is reached.)

Methodology and case studies

Sensor degradation study

Problem description and simulation procedure

Sensor degradation can result in an error growth and possible sensor failure. Two typical measurement error types are noise and drift. In this work, we evaluate quantitatively the effects these errors have on the estimation of flowrates when using a VFM scheme. This was performed explicitly by randomly varying the measurement values within a pre-defined error band. In addition, we study the effect of the sensors failure. As such, we consider the following case studies:

- Case 1: Effect of noise increase in pressure and temperature sensors
- Case 2: Effect of sensor drift in pressure and temperature sensors
- Case 3: Effect of the temperature sensors failure

The problem in all the cases is the fact that we never know the exact value of the measured quantity. Due to noise, the measurement can have any value within the sensor accuracy. Thus, to evaluate the potential spread of VFM flowrate estimates due to the measurement error, we evaluate the random combinations of pressure and temperature measurement values within specified accuracy. Since each simulation takes a considerable computational time due to the optimization routine, we cannot run a very large number of simulations. Therefore, it is decided to run 200 simulations for each sub-case (which are discussed in details in the next section) and evaluate the flowrates' probability distributions using a statistical analysis.

Fig.3 shows the simulation procedure for the sensor degradation study. To generate a good initial guess of the flowrate estimate, first, we compute the maximum and minimum possible values of pressures and temperatures. These values are computed from the sensor accuracy range. For instance, if the actual pressure value is 100 bar and the noise error is 1%, the minimum pressure value is 99 bar and the maximum value is 101 bar. These values are used to estimate the maximum and minimum possible flowrates which are averaged for the initial guess to the optimization algorithm. Starting from the initial guess, the system iteratively finds the mass flowrate which makes the difference between the VFM predictions and the wellhead temperature and bottomhole pressure to reach a minimum. The mass flowrate is used for tuning instead of the volumetric flowrates due to the limitations in the commercial multiphase flow simulator employed.

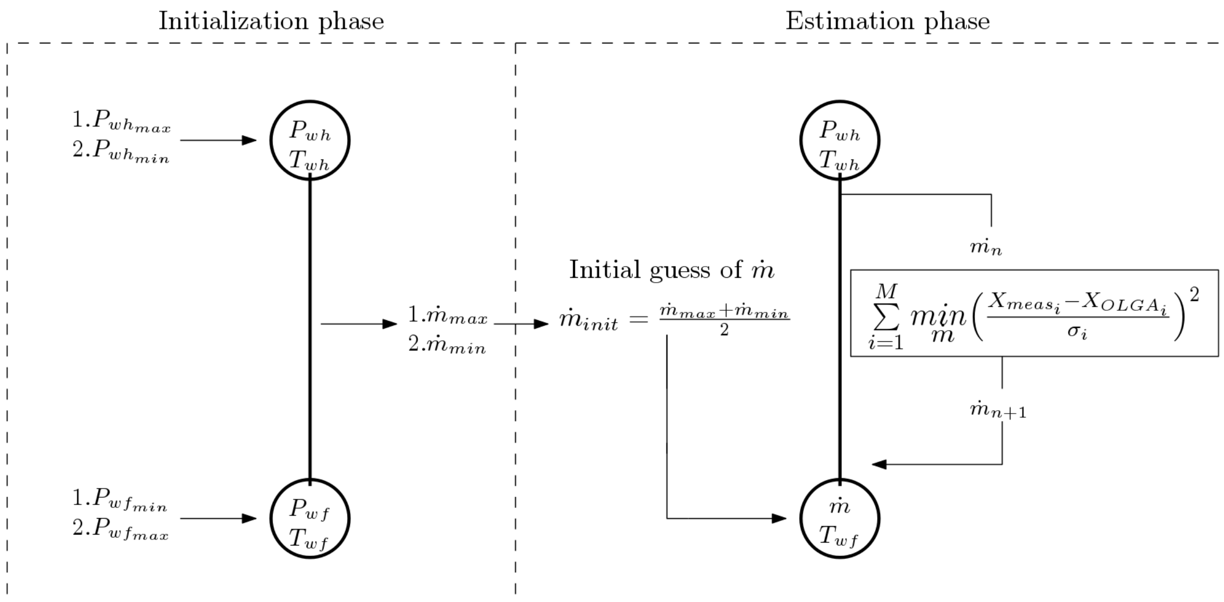

Fig. 3 – Simulation procedure for the sensor degradation study

(In the initialization phase, we compute the maximum and minimum measurement values from the accuracy range which are used to estimate maximum and minimum possible flowrates. These flowrates are averaged to generate a good initial guess of the flowrate for the estimation phase. In the estimation phase, the flowrate is iteratively adjusted by the optimizer until the cost function reaches the minimum.)

Case 1 (Effect of measurement noise)

To study the effect of noise on the VFM estimates, we consider three cases:

- Case 1.1: 0.5% noise error – base case
- Case 1.2: 1% noise error
- Case 1.3: 1.5% noise error

The main goal is to quantify the effect of the magnitude of the signal variation band on the flowrate estimates. As such, we do not consider noise filtering because even the filtered signal will have the deviation error which can increase due to the degradation.

The value of the error (0.5%, 1% or 1.5%) represents the maximum possible error in the measurements. For instance, if the actual pressure value is 100 bar and the noise error is 1%, the possible measurement readings are within the interval of 99-101 bar.

Case 1.1 is considered as the base case meaning that the sensors are newly installed and not affected by the degradation. It is worth to mention that this case will be used in other case studies as a base line for comparison. The degradation effect is modeled in Cases 1.2 and 1.3. **Fig. 4** shows an example of the signal under the modeled noise error. The error is randomly introduced to pressure and temperature measurements at the wellhead and bottomhole at the same time.

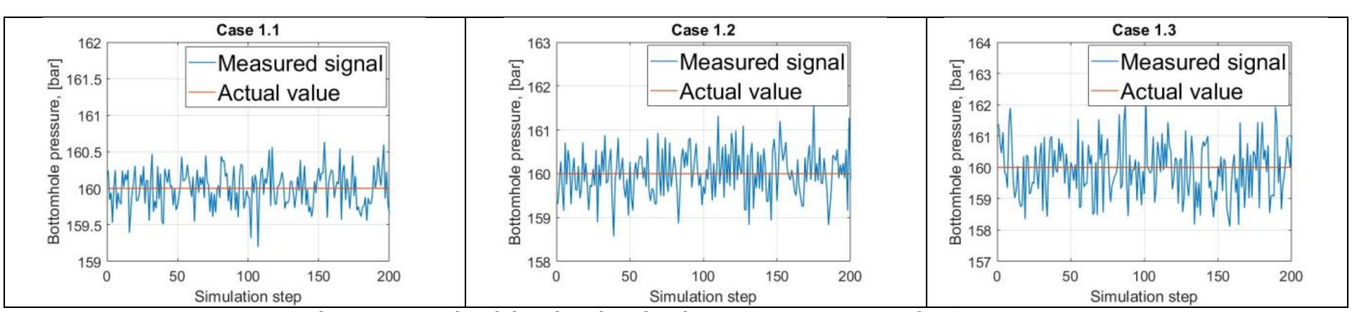

Fig. 4 – Example of the signal under the measurement error for Cases 1.x

Case 2 (Effect of measurement drift)

To model the effect of sensor drift, we consider the following cases:

- Case 2.1: 0.5% drift with 0.5% noise error
- Case 2.2: 1% drift with 0.5% noise error
- Case 2.3: 1.5% drift with 0.5% noise error

All the cases are compared with the Case 1.1 which considers the newly installed equipment. **Fig. 5** shows an example of the signal under the modeled drift error. The value of the drift (0.5%, 1% or 1.5%) represents the relative difference of the sensor value to the actual measurement value. For instance, if the actual pressure value is 100 bar and the drift error is 1%, the drifted measurement is 101 bar. Due to the noise, the final value of measurement will be within the range of 100.5-101.5 bar. The error is randomly introduced to pressure and temperature measurements at the wellhead and bottomhole at the same time. Please note that we considered only the drift which increased the measurement values and did not considered decreased values.

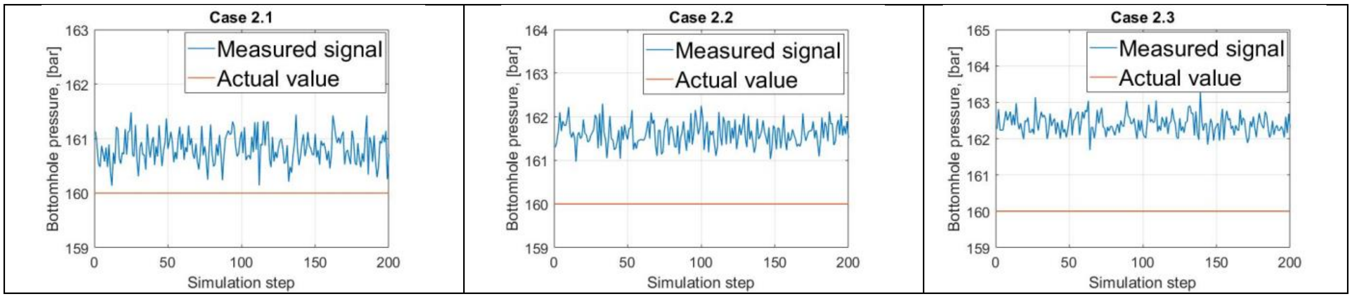

Fig. 5 – Example of the signal under the measurement error for Cases 2.x

Case 3 (Effect of temperature sensors failure)

In this case, we study the effect of the temperature sensors failure, both at the bottomhole and the wellhead. We assume that at some point of the production time the temperature sensors are degraded down to the state when the information from the sensors are unreliable or no longer available. This is a difficult case from the operational point of view because it can be challenging to identify that the sensor shows unreliable information. We do not consider the identification methods and leave it for experienced operators. What we would like to consider is the effect of the broken sensor on the VFM estimates.

When compositional model is used in the VFM system, we need to use temperature to compute the multiphase flow. In case of the sensor failure, one solution can be using the last reliable value of the temperature for the VFM system. In this case, two situations are possible:

- Case 3.1: The temperature sensors fail and the actual temperature does not change
- Case 3.2: The temperature sensors fail and the actual temperature changes

Since we concluded that we do not have the information from the temperature sensors or the information is unreliable, we exclude it from the cost function and use the last reliable value of the temperature in the inflow mass source. As such, the cost function includes only the values of the measured bottomhole pressure. In Case 3.2, we assume that the actual temperature drops by 5 ^oC, however, the VFM does not capture this because the correct temperature measurement is not available. To quantify the effect of the sensors failure, we compare these cases with Case 1.1 (no degradation).

Heat transfer modeling study

Theory and case study description

In VFM systems, in addition to the flowrate, matching the temperature measurements in the well can be achieved by adjusting the heat transfer coefficient. The overall heat transfer coefficient U is a constant between the thermal flux and the temperature difference of two mediums which can be expressed as:

$$U = \frac{Q}{A\left(T_f - T_{amb}\right)} \tag{2}$$

where Q denotes the heat flux, A – the heat transfer area, T_f – fluid temperature, T_{amb} – ambient (formation) temperature.

Considering the well structure in Fig.1, the heat transfer between the formation and the multiphase flow for each well section can be written as:

$$Q_j = 2\pi R_{inner} L_{\sec} h_{inner}\left(T_f - T_w\right) + \sum_{i=1}^{n} \frac{2\pi R_{inner} L_{\sec} K_j \left(T_{outer\ j} - T_{inner\ j}\right)}{\ln \frac{R_{outer\ j}}{R_{inner\ j}}} + \frac{2\pi L_{\sec} K_{form}\left(T_{cem} - T_{amb}\right)}{T_{D_{\sec}}} \tag{3}$$

where R_{inner} denotes the inner tubing radius, $R_{inner\,j}$ – the inner radius of the *j-th* layer, $R_{outer\,j}$ – the outer radius of the *j-th* layer, h_{inner} – the convective heat transfer coefficient, T_w – the wall temperature, K_j – the thermal conductivity of the *j-th* layer, L_{sec} – the section length, T_{cem} – the cement temperature, K_{form} – the formation thermal conductivity, T_{Dsec} – the dimensionless temperature of the section.

The terms in Eq.3 respectively represent the following heat transfer mechanisms:

- Convective heat transfer between the fluid and the tubing wall
- Heat conduction between the walls and mud/cement
- Heat conduction between the outer casing wall and the formation

By substituting the left hand side of Eq.3 by Eq.2 taking into account the well mechanical structure of each section from Fig.1 and solving it with respect to U, the following equations for can be obtained:

$$\frac{1}{U_1} = \frac{1}{h_{inner}} + \frac{R_{17}}{K_{mud}}\left[\ln\left(\frac{R_{12}}{R_{16}}\right) + \ln\left(\frac{R_9}{R_{11}}\right) + \ln\left(\frac{R_6}{R_8}\right)\right] + \frac{R_{17}}{K_w}\left[\ln\left(\frac{R_{16}}{R_{17}}\right) + \ln\left(\frac{R_{11}}{R_{12}}\right) + \ln\left(\frac{R_8}{R_9}\right) + \ln\left(\frac{R_5}{R_6}\right) + \ln\left(\frac{R_2}{R_3}\right)\right] + \frac{R_{17}}{K_{cem}}\left[\ln\left(\frac{R_3}{R_5}\right) + \ln\left(\frac{R_1}{R_2}\right)\right] + \frac{T_{D1}R_{17}}{K_{form}} \tag{4}$$

$$\frac{1}{U_2} = \frac{1}{h_{inner}} + \frac{R_{17}}{K_{mud}}\left[\ln\left(\frac{R_{12}}{R_{16}}\right) + \ln\left(\frac{R_9}{R_{11}}\right) + \ln\left(\frac{R_6}{R_8}\right)\right] + \frac{R_{17}}{K_w}\left[\ln\left(\frac{R_{16}}{R_{17}}\right) + \ln\left(\frac{R_{11}}{R_{12}}\right) + \ln\left(\frac{R_8}{R_9}\right) + \ln\left(\frac{R_5}{R_6}\right)\right] + \frac{R_{17}}{K_{cem}}\left[\ln\left(\frac{R_4}{R_5}\right)\right] + \frac{T_{D4}R_{17}}{K_{form}} \tag{5}$$

$$\frac{1}{U_3} = \frac{1}{h_{inner}} + \frac{R_{17}}{K_{mud}}\left[\ln\left(\frac{R_{12}}{R_{16}}\right) + \ln\left(\frac{R_9}{R_{11}}\right)\right] + \frac{R_{17}}{K_w}\left[\ln\left(\frac{R_{16}}{R_{17}}\right) + \ln\left(\frac{R_{11}}{R_{12}}\right) + \ln\left(\frac{R_8}{R_9}\right)\right] + \frac{R_{17}}{K_{cem}}\left[\ln\left(\frac{R_7}{R_8}\right)\right] + \frac{T_{D7}R_{17}}{K_{form}} \tag{6}$$

$$\frac{1}{U_4} = \frac{1}{h_{inner}} + \frac{R_{17}}{K_{mud}}\left[\ln\left(\frac{R_{12}}{R_{16}}\right)\right] + \frac{R_{17}}{K_w}\left[\ln\left(\frac{R_{16}}{R_{17}}\right) + \ln\left(\frac{R_{11}}{R_{12}}\right)\right] + \frac{R_{17}}{K_{cem}}\left[\ln\left(\frac{R_{10}}{R_{11}}\right)\right] + \frac{T_{D10}R_{17}}{K_{form}} \tag{7}$$

$$\frac{1}{U_5} = \frac{1}{h_{inner}} + \frac{R_{17}}{K_{mud}}\left[\ln\left(\frac{R_{15}}{R_{16}}\right)\right] + \frac{R_{17}}{K_w}\left[\ln\left(\frac{R_{16}}{R_{17}}\right) + \ln\left(\frac{R_{14}}{R_{15}}\right)\right] + \frac{R_{17}}{K_{cem}}\left[\ln\left(\frac{R_{13}}{R_{14}}\right)\right] + \frac{T_{D13}R_{17}}{K_{form}} \tag{8}$$

where K_{cem} denotes the thermal conductivity of the cement, K_{mud} – the thermal conductivity of the mud.

In VFM systems, the heat transfer coefficients are often used as one of the parameters to match a specific temperature, e.g. at the wellhead. A reasonable strategy can be computing initial estimates for the heat transfer coefficients using the equations above and then tune it until a satisfactory agreement between the measured and predicted temperature values is reached. This is the first method used in this study.

On the other hand, it is interesting to see if it is possible to achieve the same accuracy as in the previous case without a rigorous representation of the heat transfer. For instance, it might be assumed that the heat transfer coefficient is constant along the wellbore. In this way, only one coefficient value is tuned in VFM to reach the specific temperature. This is the second method used in this study.

As such, we consider two cases:

- Case 4.1: Tuning with multiple heat transfer coefficients
- Case 4.2: Tuning with one heat transfer coefficient

Simulation procedure

As in the sensor degradation case, we randomly choose the pressure and temperature measurement values within a specified sensor accuracy (0.5% noise error) and perform 200 simulations to compute flowrates probability distributions.

To compute the initial estimates of the heat transfer coefficients for each section in Case 4.1, we use Eqs.4-8. First, we compute the heat conduction between the outer layer and formation for each section using the last terms in Eqs.4-8. For calculating the dimensionless temperature T_D, the correlation by Hasan and Kabir (2012) is used:

$$T_D = \ln\left[e^{-0.2t_D} + (1.5 - 0.3719 \cdot e^{-t_D})\sqrt{t_D}\right] \tag{9}$$

$$t_D = \frac{a \cdot t}{R^2_{outer\ i}} \tag{10}$$

where t_D denotes the dimensional producing time, a – the formation heat diffusivity, t – producing time.

For the producing time t, we chose 100 days assuming that this is sufficient for the heat transfer between the fluid and the formation to reach a steady state.

Secondly, we calculate the heat conduction between the casing walls and cement/mud. In each section, the number of layers of the well structure varies which makes these values different from one section to another.

An order of magnitude analysis showed that the inner convection heat transfer between the multiphase flow and the tubing has a little contribution to the heat transfer between the flow and formation. Therefore, we do not include it into the final simulation procedure.

One important thing to mention is the fact that we keep the ratio between the heat transfer coefficients constant when tuning the VFM and use it as constraints in the optimization procedure. This is because we would like to achieve the original pattern of the heat transfer distribution along the wellbore. Otherwise, there might be the case that the algorithm changes one coefficient more than the others, so that the actual heat flux distribution will be changed to something less realistic.

The summary of the simulation procedure is shown in **Fig. 6**. In the initialization phase, the computed values of the heat transfer coefficients from Eqs.4-8 used as an initial guess and tuned until a specific wellhead temperature is matched. Then, the tuned coefficient values are used as an initial guess for the simulation phase and further adjusted together with the mass source to fit specific pressure and temperature values. The same procedure is used for the single heat transfer coefficient case except the fact that the initial coefficient value is guessed rather than preliminary computed. The computational procedure for the single heat transfer coefficient case is shown in **Fig.7**.

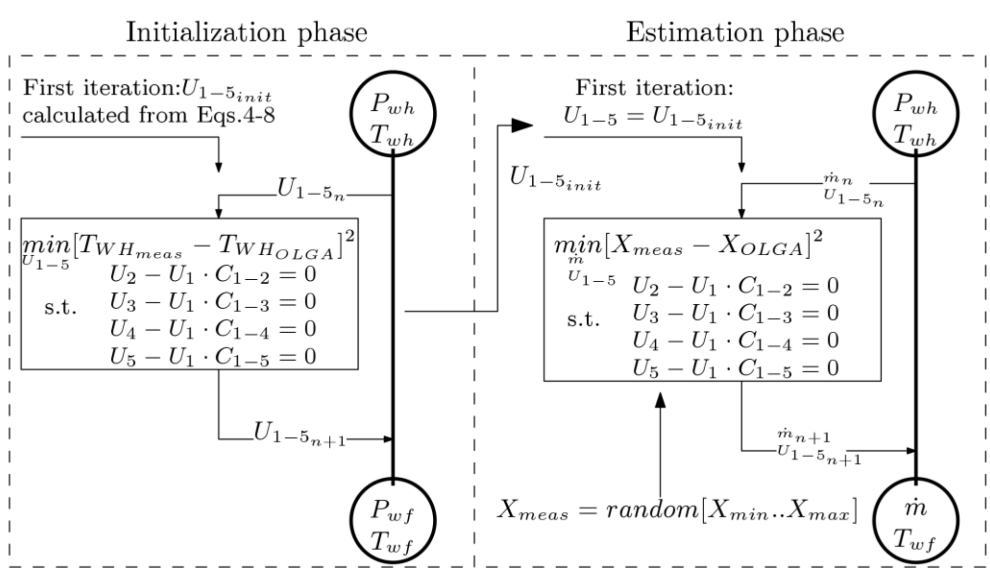

Fig.6 – Schematic simulation procedure for Case 4.1 (multiple heat transfer coefficient tuning)

(In the initialization phase, we compute the initial values of the heat transfer coefficients using Eqs.4-8 and then iteratively adjust these values until a good match of the wellhead temperature is reached. The obtained values are used as a good initial guess for the estimation phase where the heat transfer coefficients are tuned together with the mass flowrate to reach pressure and temperature values at the wellhead and bottomhole. The ratios between the heat transfer coefficients are kept constant and specified as constraints in the optimization problem.)

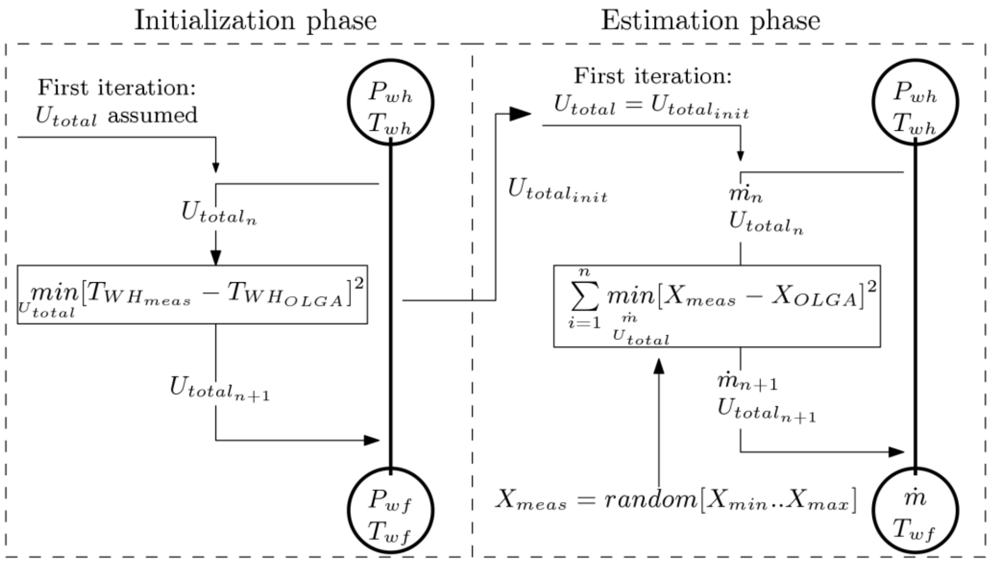

Fig.7 – Schematic simulation procedure for Case 4.2 (single heat transfer coefficient tuning)
(In the initialization phase, we make an assumption of the heat transfer coefficient and then iteratively adjust this value using the optimizer until a good match of the wellhead temperature is reached. The obtained value is used as a good initial guess for the estimation phase where the heat transfer coefficient is tuned together with the mass flowrate to reach pressure and temperature values at the wellhead and bottomhole.)

Statistical analysis

To analyze the simulations results, we perform a statistical analysis of the resulting flowrate distributions taken from 200 simulations of each case. We use the following procedure:

1. Test data normality.
2. Compute appropriate parameters for statistical and practical significance evaluation (mean/median, standard deviation (variance)/interquartile range).
3. Perform hypothesis testing to test the statistical significance of the results.
4. Evaluate the practical significance of the results.

In step 1, we test the data normality to select the appropriate strategy to compare the data samples. For this purpose, we perform a visual analysis using Q-Q plots and use D’Agostino test to check the normality formally. The Q-Q plot is a graphical method for checking the data normality by plotting quantiles of two distributions in which one distribution is normal. D’Agostino test is a formal statistical test of the data normality which was developed for sample sizes larger than 50 (D'Agostino 1971). In this study, we consider the significance level to be 0.05 which is a common assumption in staistical analysis.

In step 2, when the normality test is completed, we compute the parameters for statistical and practical significance evaluation of the samples. If the data is normally distributed, we select mean and variance for statistical significance evaluation and mean and standard deviation for practical significance evaluation. This is because the standard deviation has the units of the variable evaluated, so that it is easier to interpret the results for practical purposes. If the data is non-normal, we compute median and interquartile range be these parameters can be more representative than mean and standard deviation for this type of data.

In step 3, we perform hypothesis tests to check the statistical difference between the simulated cases. These tests provide an opportunity to check if the differences between the statistical properties of the data samples can be generalized over the populations from which these samples are taken. If the data is normally distributed, we choose 1-sample t-test on paired data differences. The reason for selecting 1-sample test instead of 2-samples test is because the samples are dependent. Indeed, initially we consider a system without the degradation effect and then we consider the same system under the degradation. To compare the variances, Bartlett’s test is used (Snedecor and Cochran 1989). If the data is non-normal, we compare the medians using 1-sample sign test on paired differences and variances using Levene's test (Levene 1960).

Finally, in step 4, if we find that the difference between the parameters is statistically significant, we evaluate the practical significance of the obtained results. The evaluation of the practical significance will depend on the case under consideration. In general, we will compare differences of the means or standard deviations (or medians and interquartile ranges) as fractions of the mean estimate as well as the absolute differences values. **Fig. 8** summarizes the used statistical analysis.

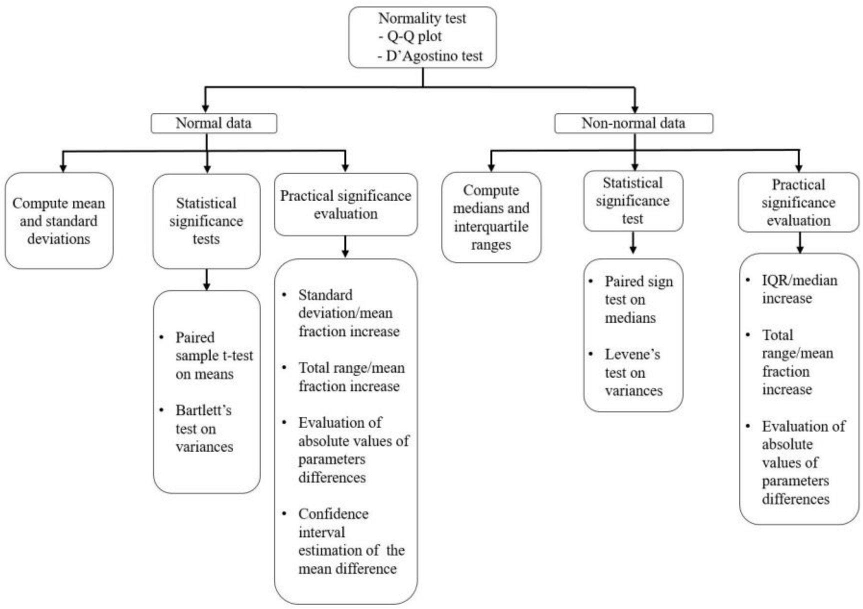

Fig.8 –Schematic representation of the statistical analysis

Results

Sensor degradation

Case 1

First, we analyze the case with the increased noise effect due to sensor degradation. **Fig. 9** shows the obtained oil and gas flowrate distributions.

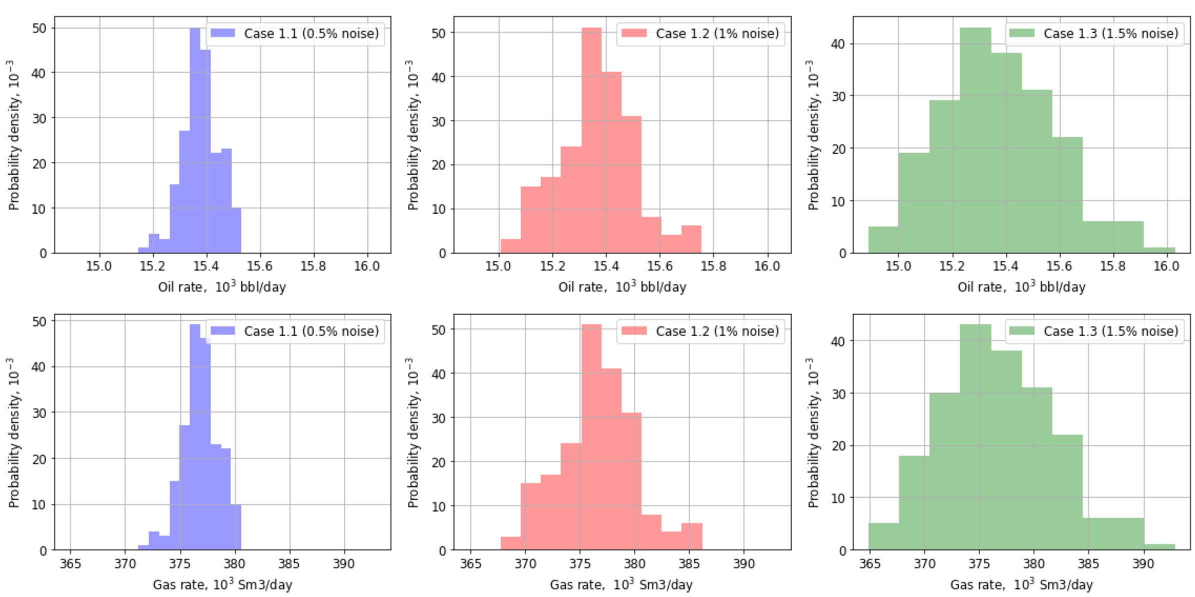

Fig.9 – Histograms of VFM flowrate predictions for Cases 1.x

From the figure we see that the respective oil and gas flowrates are represented by the same distribution. This is expected because the volumetric flowrates are computed from the same mass flowrate source by means of a linear transformation. From the figure we can also notice that data is not precisely normal even though the input signals have white noise. The reason for this is the fact that the system is non-linear which can make the output signals to have a different distribution. However, the data might still be considered as normal and must be checked for normality to make valid conclusions. Also, the initial visual analysis shows that the increase of the noise make the distribution more spread, i.e. increases the data variability. This result was expected. However, the main goal is to quantify this data variability growth and generalize the conclusions for the populations from which the samples are taken.

To perform further analysis, we check the data normality. **Fig. 10** shows the visual and formal analysis represented by the Q-Q plots with corresponding p-values from the D'Agostino tests.

From the Q-Q plots we see that the majority of the data points follow the normal distribution pattern (red line) except a few points. This confirms the visual observations from Fig. 9 that the data is close to normal. By checking the normality formally by D'Agostino test, we cannot reject the null hypothesis that the data is normal at the significance level of 0.05 which is in agreement with the visual analysis.

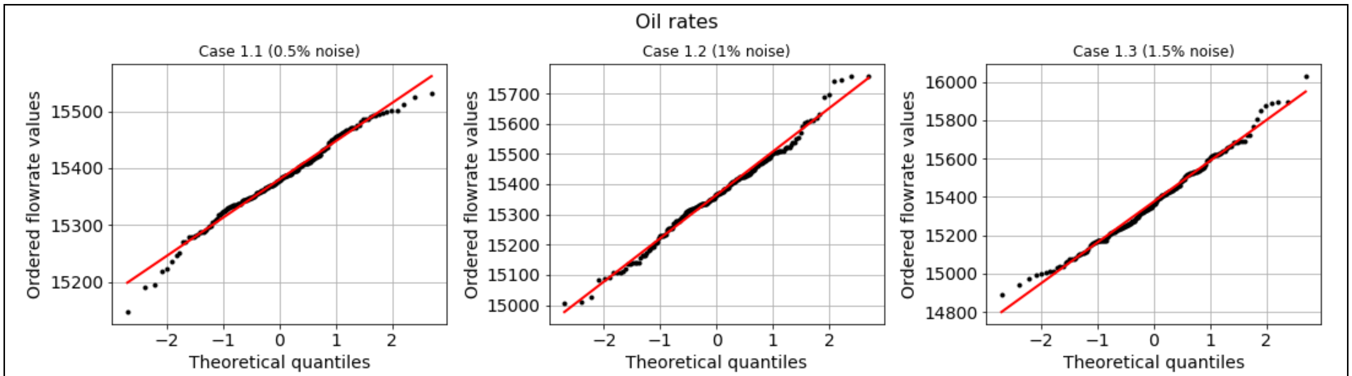

D'Agostino p-value = 0.086	D'Agostino p-value = 0.485	D'Agostino p-value = 0.193

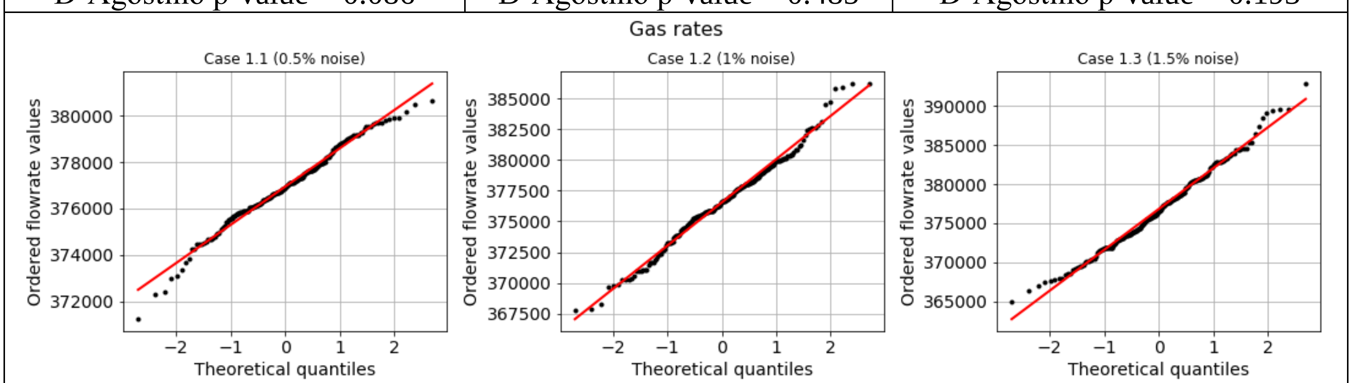

D'Agostino p-value = 0.083	D'Agostino p-value = 0.48	D'Agostino p-value = 0.194

Fig. 10 – Normality testing of datasets from Cases 1.x

Since we conclude that the data can be considered as normal, we choose means and standard deviations as measures for the central distribution value and data variability respectively. We also consider the total variation of the flowrate estimates to compare the resulting distributions. **Table 1** shows the values of these data.

From the table we see that the estimates of the means are similar while the variation of the standard deviations is much larger. Now we need to test if these differences are statistically significant. **Table 2** shows the differences of means, standard deviations and total ranges between the cases as well as the results from the hypothesis tests on the means and variances equalities.

	Oil rates		
	Case 1.1	Case 1.2	Case 1.3
Mean, bbl/day	15380.02	15364.14	15374.91
Standard deviation, bbl/day	66.94	130.54	211.32
Total range, bbl/day	384.33	729.40	1141.18
	Gas rates		
	Case 1.1	Case 1.2	Case 1.3
Mean, Sm3/day	376940.80	376517.49	376814.36
Standard deviation, Sm3/day	1640.14	3201.04	5182.83
Total range, bbl/day	9418.93	17903.42	27990.72

Table 1 – Main statistical parameters of the simulation results of Cases 1.x

Parameter/Hypothesis	Case1.1 and Case 1.2	Case 1.1 and Case 1.3
	Oil rates	
Sample means difference, bbl/day	15.87	5.1
t-test p-value (H_0: $mean_1$=$mean_2$)	0.16	0.75
Standard deviation difference, bbl/day	75.53	144.39
Total range difference, bbl/day	365.5	756.84
Bartlett's test p-value (H_0: var_1 = var_2)	$2.15 \cdot 10^{-24}$	$1.36 \cdot 10^{-49}$
	Gas rates	
Sample means difference, Sm3/day	389.64	126.44
t-test p-value (H_0: $mean_1$=$mean_2$)	0.16	0.75
Standard deviation difference, Sm3/day	1853.55	3542.7
Total range difference, Sm3/day	8991.06	18571.78
Bartlett's test p-value (H_0: var_1 = var_2)	$1.93 \cdot 10^{-24}$	$1.17 \cdot 10^{-49}$

Table 2 – Hypothesis testing and comparison of statistical parameters of Cases 1.x

From the table we can make several conclusions. First, we see that based on this study we cannot reject the null hypothesis about the means equalities at the significance level of 0.05. Thus, we conclude that there is no statistically significant difference between the population means which, in turn, tells that the population means can be considered as equal. This seems to be in agreement with the practical significance of the results. The difference in the means varies from 5.1 to 15.87 bbl/day which in practice can be neglected. Therefore, for practical purposes, we can say that if the sensor degradation affects the noise level only, the means of the flowrates estimates are not affected significantly. We see an opposite situation for the data variability. Comparing the statistical significance of the variance differences (Bartlett's test), we see that the null hypothesis is strongly rejected, which means that the populations variances are certainly different.

To estimate the practical significance of variance differences, we compare the absolute and relative values of the standard deviations and total ranges. The relative values are scaled with respect to the means. **Fig.11** and Table 2 show that the increase of the measurement error by 0.5% causes the increase of the standard deviation and the total range by approximately 76 bbl/day and 366 bbl/day respectively. These values can be considered as significant. However, as Fig. 11 shows, these values correspond approximately to 0.5% and 2.5% of the mean flowrate value respectively. In certain VFM applications this error might be neglected, however, if the desired accuracy of the flowrate estimation is high, the increase of the measurement noise can cause problems in meeting the aimed accuracy specification. Moreover, the considered measurement error is relatively small, so that for larger measurement variations the associated error can be noticeable. As such, we conclude that the found standard deviation difference is practically significant if the desired accuracy of VFM is high or the noise error is relatively large but can be neglected in other situations. This is because the obtained absolute values are small when scaled with respect to the mean value estimate. The same conclusions can be drawn for the gas rates because we observed that its distribution pattern is the same as for the oil rates.

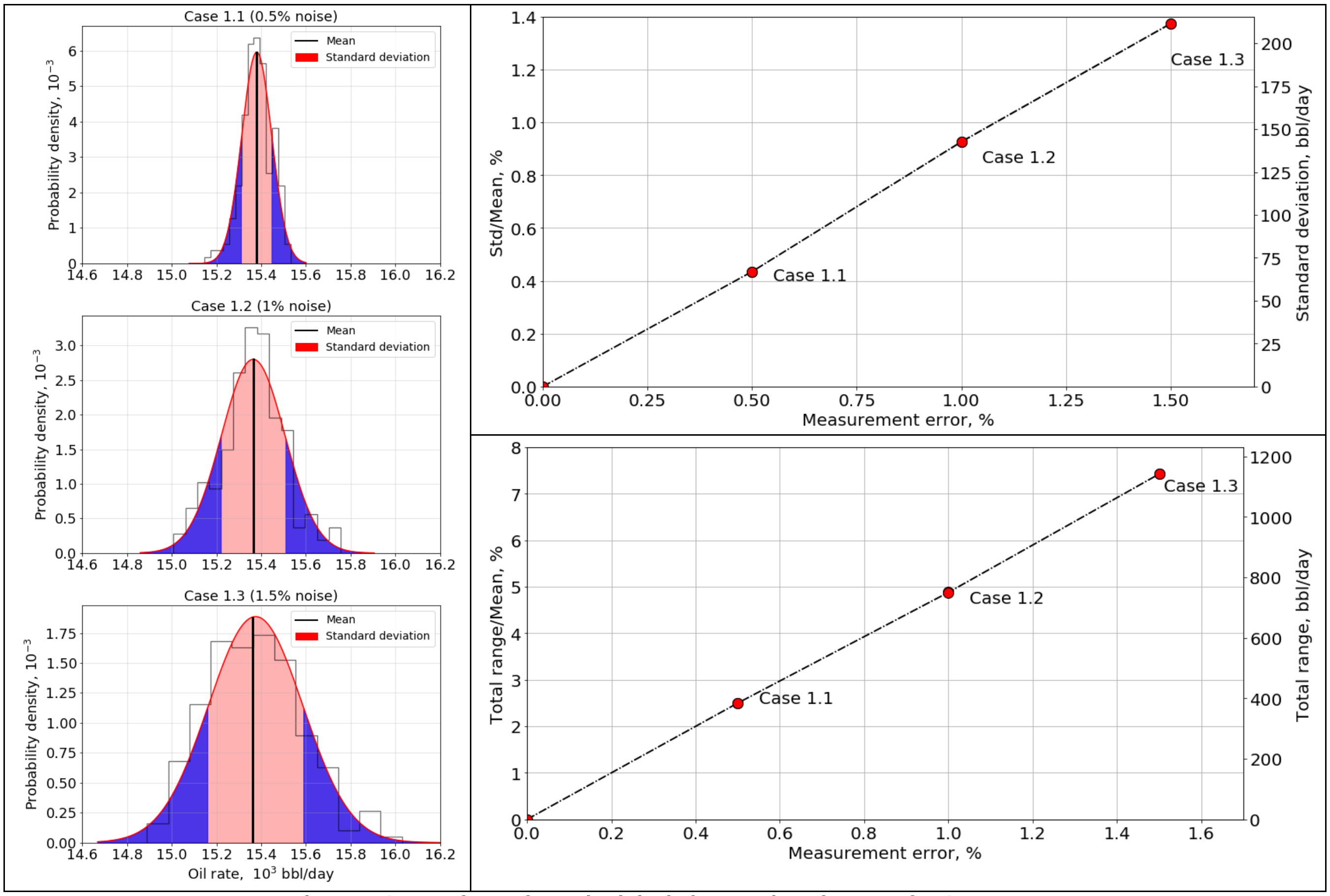

Fig. 11 – Comparison of standard deviations and total ranges for Cases 1.x

(The left part of the figure visualizes the increase of the data variability depending on the increase of the noise level. The figures on the right quantify this data variability increase. We can see that even though the increase of the standard deviation and total range is relatively big from Case 1.1 to Case 1.2 and Case 1.3, these values may be neglected in many practical applications since they are small fractions of the mean flowrate estimate unless the noise level becomes relatively large.)

Case 2

As the next step, we analyze the effect of measurement drift on the flowrate estimates from the VFM. **Fig. 12** shows the oil and gas flowrate distributions. As in the previous case, the respective oil and gas flow rates are represented by the same distribution. As expected, we see a similar data variability between the cases but the migration of the mean value. This is because the noise level is kept the same for all the cases while the mean measurement value is different. Now the task is to evaluate the mean differences from statistical and practical points of view.

First, we check the datasets normality. **Fig. 13** shows the visual and formal analysis represented by the Q-Q plots with corresponding p-values from the D'Agostino tests. As in the previous case, we see that the majority of the data points follow the normal distribution pattern (red line) except a few points. This suggests that the data is close to normal. By checking the normality formally with D'Agostino test, we cannot reject the null hypothesis that the data is normal at the significance level of 0.05 and assume that the data can be treated as normal.

The next step is to compute the means, standard deviations and total ranges of the estimates. **Table 3** shows the values of these parameters. From the table we see that the computed standard deviations are similar while the means vary considerably. This is in agreement with what we observed in Fig.12. **Table 4** shows the differences of means, standard deviations and total ranges between the cases as well as the results from the hypothesis tests on the means and variances equalities.

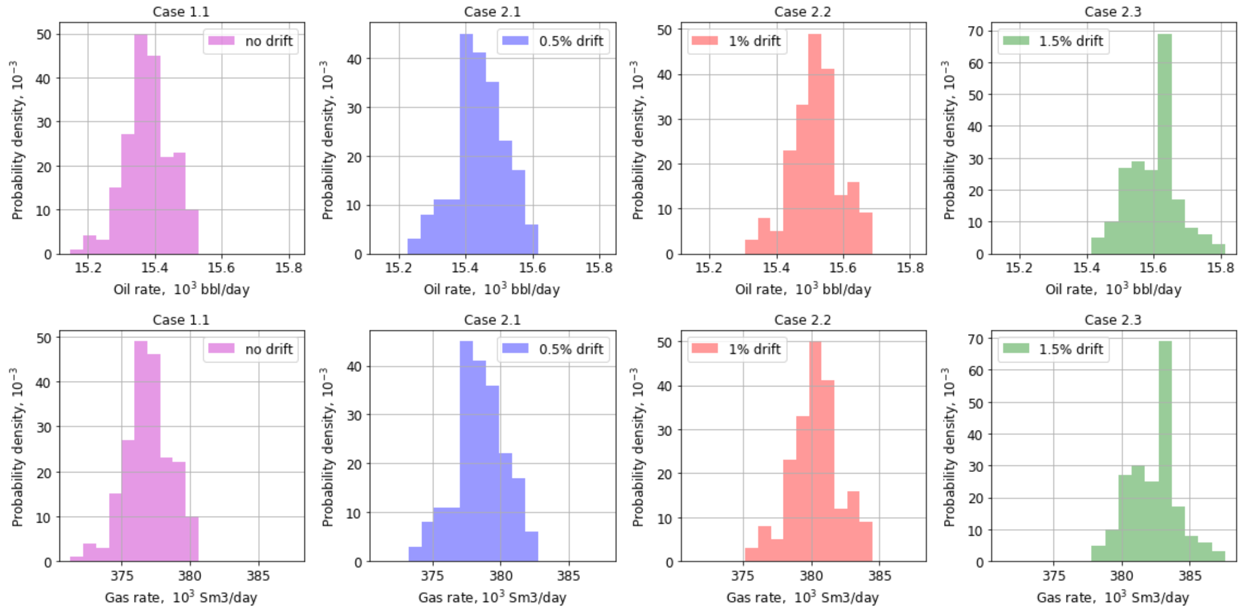

Fig.12 – Histograms of VFM flowrate predictions for Cases 2.x and Case 1.1

From the table we see that the hypothesis of the equal mean values is strongly rejected, thus we conclude that the population means are certainly different. As for the variances, the hypothesis of its equalities cannot be rejected which means that the variances of the populations are not statistically different at the significance level of 0.05. As such, from the analysis we see that only the means are affected by the measurement drift and the next objective is to estimate the practical importance of the means differences. **Fig.14** shows the comparison of the means differences relative to the mean of Case 1.1.

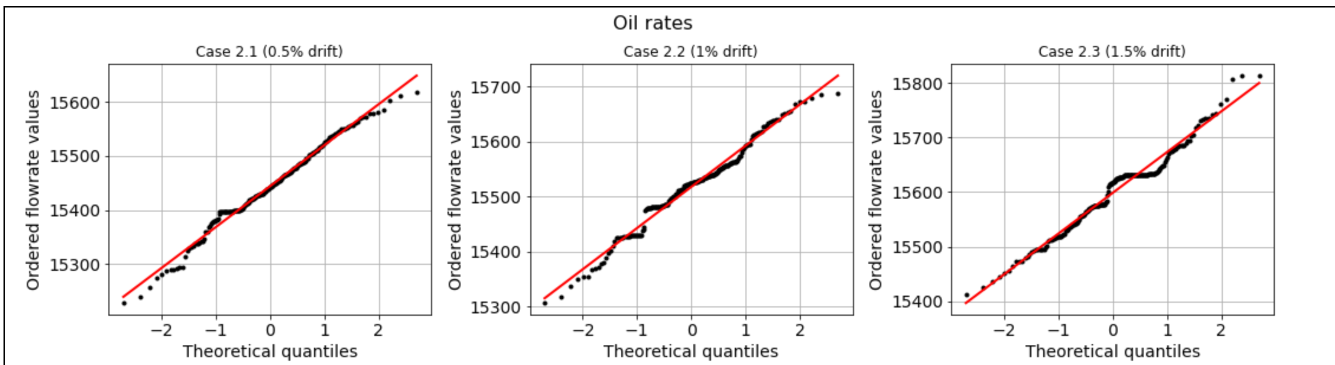

D'Agostino p-value = 0.39	D'Agostino p-value = 0.49	D'Agostino p-value = 0.41

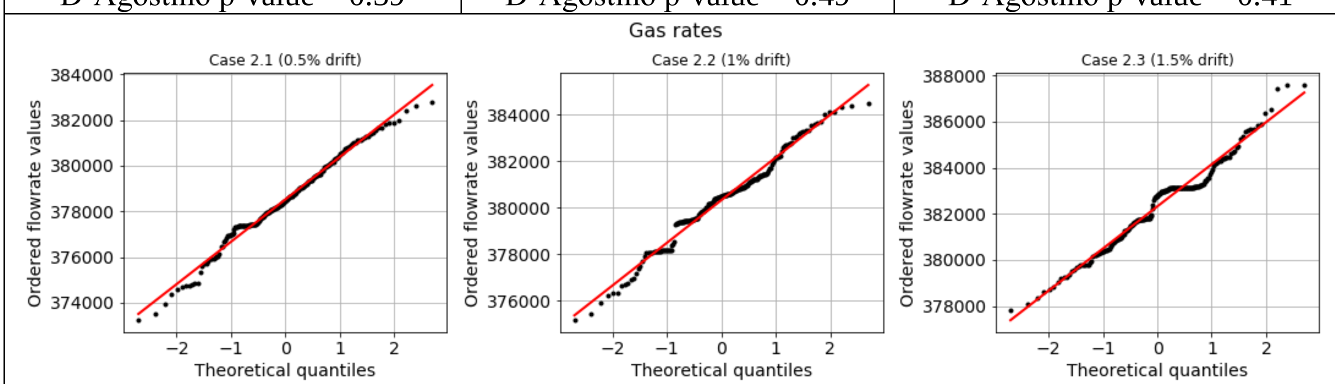

D'Agostino p-value = 0.4	D'Agostino p-value = 0.49	D'Agostino p-value = 0.41

Fig. 13 – Normality testing of datasets from Cases 2.x

	Oil rates		
	Case 2.1	Case 2.2	Case 2.3
Mean, bbl/day	15444.1	15517.55	15598.33
Standard deviation, bbl/day	75.31	74.54	74.58
Total range, bbl/day	390.39	380.52	399.66
	Gas rates		
	Case 2.1	Case 2.2	Case 2.3
Mean, Sm3/day	378520.31	380331.15	382320.24
Standard deviation, Sm3/day	1846.54	1827.3	1837.02
Total range, bbl/day	9569.27	9331.26	9791.52

Table 3 – Main statistical parameters of the simulation results of Cases 2.x

Parameter/Hypothesis	Case1.1 and Case 2.1	Case 1.1 and Case 2.2	Case 1.1 and Case 2.3
	Oil rates		
Sample means difference, bbl/day	64.06	137.54	218.34
95% confidence interval of the means difference, bbl/day	[52.4 – 75.74]	[126.68 – 148.4]	[203.89 – 232.74]
t-test p-value (H_0: $mean_1=mean_2$)	$8.81 \cdot 10^{-22}$	$3.10 \cdot 10^{-63}$	$2.15 \cdot 10^{-75}$
Standard deviation difference, bbl/day	8.37	7.61	7.65
Total range difference, bbl/day	6.05	3.82	15.33
Bartlett's test p-value (H_0: $var_1 = var_2$)	0.097	0.13	0.13
	Gas rates		
Sample means difference, Sm3/day	1579.51	3390.35	5379.44
95% confidence interval of the means difference, bbl/day	[1293.63 – 1865.39]	[3124.13 – 3656.56]	[5025.57 – 5733.27]
t-test p-value (H_0: $mean_1=mean_2$)	$5.58 \cdot 10^{-22}$	$1.30 \cdot 10^{-63}$	$9.69 \cdot 10^{-76}$
Standard deviation difference, Sm3/day	206.41	187.16	189.19
Total range difference, Sm3/day	150.33	87.68	372.58
Bartlett's test p-value (H_0: $var_1 = var_2$)	0.095	0.128	0.124

Table 4 – Hypothesis testing and comparison of statistical parameters in Cases 2.x

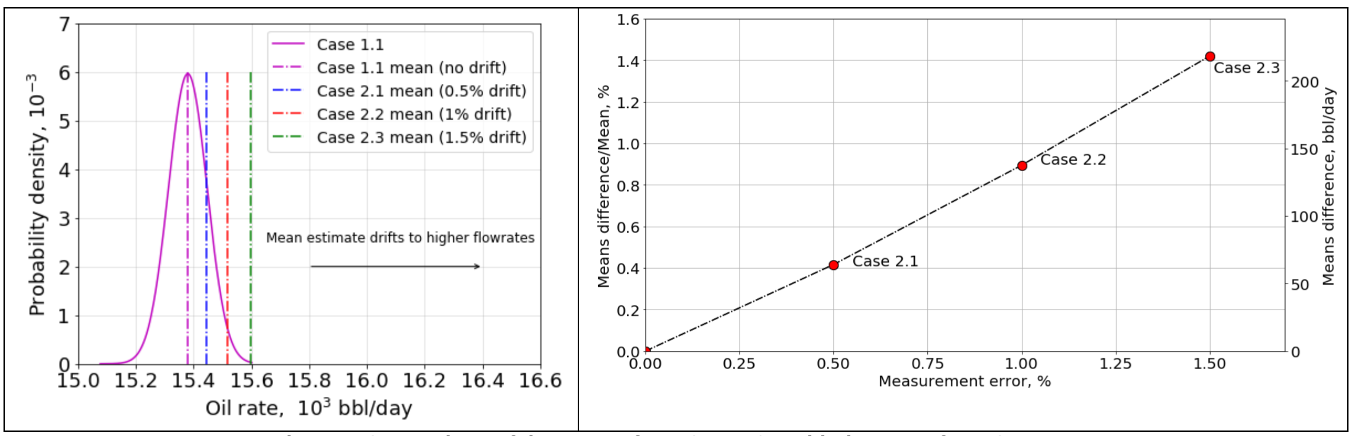

Fig. 14 – Comparison of the means from Cases 2.x with the mean from Case 1.1

(The left figure visualizes the drift of the mean estimates depending on the drift measurement error. The right figure quantifies the differences in mean estimates depending on the drift error.)

From the figure we see almost a linear relationship between the relative error of the means and the measurement error which is similar to what we previously observed for the standard deviations comparison. More specifically, the increase of the measurement error by 0.5% causes approximately 0.5% increase of the bias of the mean relative to the mean value. However, the error of the means is more critical than the error in standard deviations. This is because the probability of having a significant error of the flowrate estimates increases considerably. It can be seen in **Fig.15** where the green shaded area shows the range of the flowrates from Case 1.1 (no degradation) which can be covered by the VFM under the degradation effect. In the left figure, we see that the entire range of the flowrates of Case 1.1 is almost within the standard deviations of Case 1.3. On the other hand, only 50% of the Case 1.1 flowrates is within 50% predictions from Case 2.3. Thus, we conclude that the sensor drift causes more serious flowrate estimation errors and should be carefully considered in VFM systems.

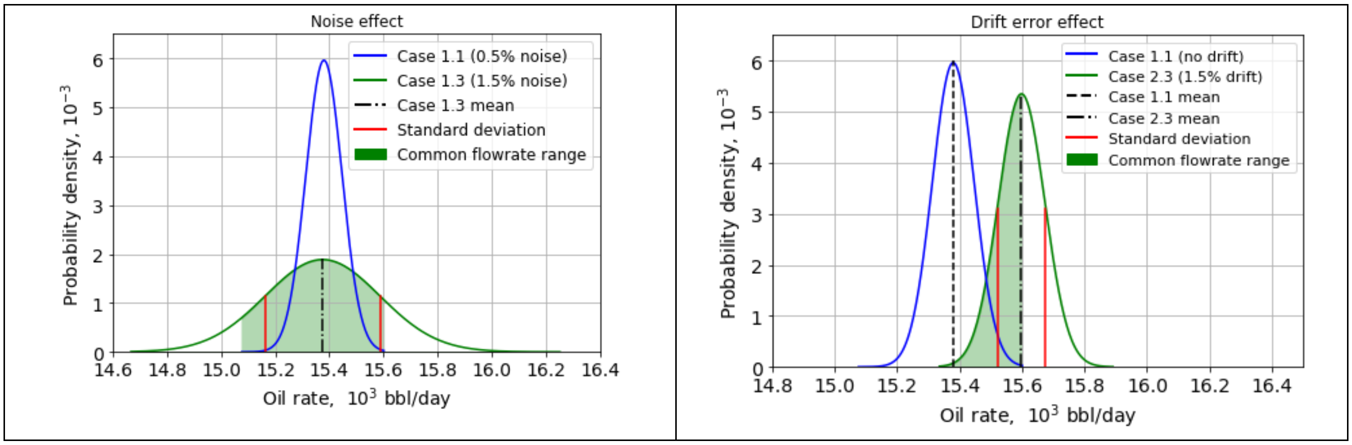

Fig.15 – Comparison of the noise and drift degradation effects

(The left figure shows that 1.5% noise error introduces the high spread of the flowrate estimations, however, the entire flowrate range of the case with no degradation is almost within the standard deviation of the case with high noise error. The right figure shows that the drift error causes significant estimation error because only 50% of the no drift case can be covered by 50% of the outcomes from the case with 1.5% drift error.)

Case 3

In this section, we compare the cases with a detected temperature sensor failure with Case 1.1 (no degradation effect). **Fig.16** shows the comparison of the flowrate distributions of these cases. From the figure we see that the absence of the temperature measurements almost does not change the flowrate distribution. However, if the actual flow temperature value changes and the VFM does not take it into account, the mean of the flowrate distribution changes considerably.

To quantify this change, again, first, we test the data normality. **Fig. 17** shows the visual and formal analysis represented by the Q-Q plots with corresponding p-values from the D'Agostino tests. Similarly to the previous cases, the analysis shows that the data can be considered as normal.

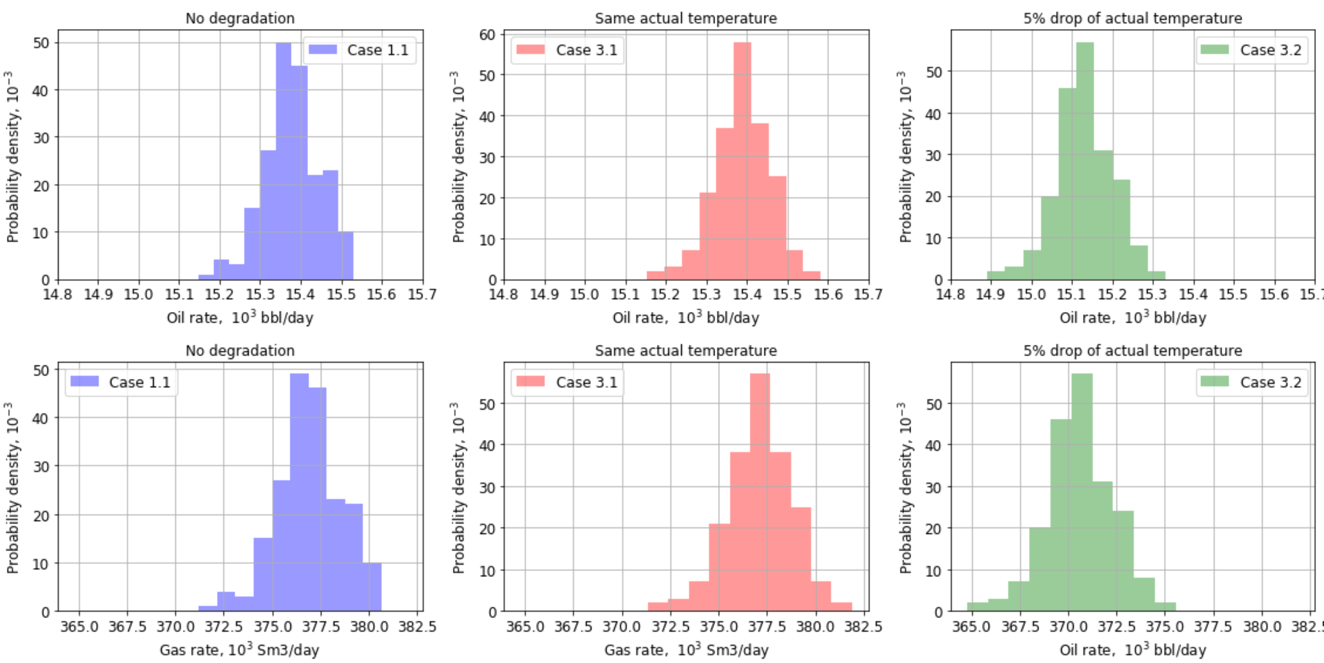

Fig. 16 – Comparison of flowrate distributions for Cases 3.x and Case 1.1

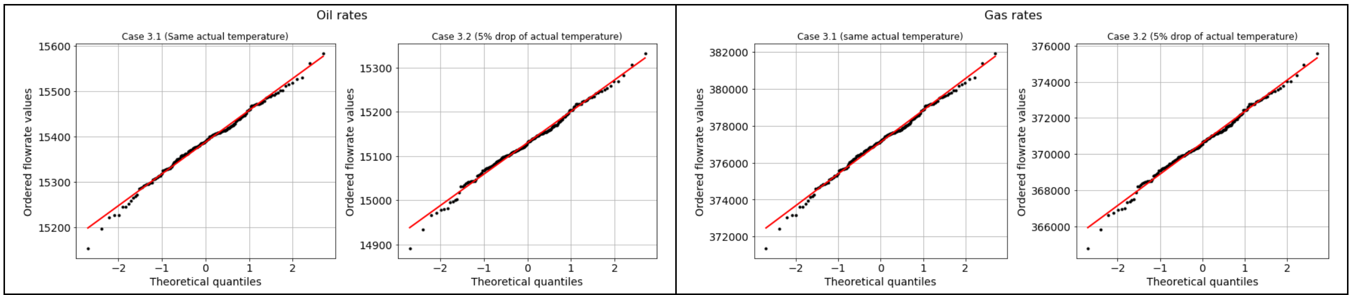

D'Agostino p-value = 0.16	D'Agostino p-value = 0.24	D'Agostino p-value = 0.16	D'Agostino p-value = 0.24

Fig. 17 – Normality testing of datasets from Cases 3.x

The next step is to compute the means, standard deviations and total ranges of the estimates. **Table 5** shows the values of these parameters.

	Oil rates	
	Case 3.1	Case 3.2
Mean, bbl/day	15386.91	15129.72
Standard deviation, bbl/day	69.6	70.46
Total range, bbl/day	429.37	440.0
	Gas rates	
	Case 3.1	Case 3.2
Mean, Sm3/day	377109.6	370621.84
Standard deviation, Sm3/day	1707.24	1727.53
Total range, bbl/day	10537	10786.84

Table 5 – Main statistical parameters of the simulation results of Cases 3.x

From the table we see that the computed standard deviations are similar to the ones in Case 1.1. On the other hand, the mean value of Case 3.2 varies considerably from Case 1.1 and Case 3.1. **Table 6** shows the differences of means and standard deviations and its statistical significance as well as the total ranges differences.

Parameter/Hypothesis	Case1.1 and Case 3.1	Case 1.1 and Case 3.2
	Oil rates	
Sample means difference, bbl/day	6.9	260.3
t-test p-value (H_0: $mean_1$=$mean_2$)	0.2	$3.01 \cdot 10^{-88}$
Standard deviation difference, bbl/day	2.67	3.53
Total range difference, bbl/day	45.04	55.67
Bartlett's test p-value (H_0: $var_1 = var_2$)	0.58	0.47
	Gas rates	
Sample means difference, Sm3/day	168.8	6318.95
t-test p-value (H_0: $mean_1$=$mean_2$)	0.2	$1.8 \cdot 10^{-90}$
Standard deviation difference, Sm3/day	206.41	187.16
Total range difference, Sm3/day	1118.13	1367.9
Bartlett's test p-value (H_0: $var_1 = var_2$)	0.57	0.46

Table 6 – Hypothesis testing and comparison of statistical parameters in Cases 3.x

From the table we see that for Case 3.1 the hypothesis of equal population means cannot be rejected while for Case 3.2 it is strongly rejected. At the same time, for both cases the hypothesis about the population variances equalities cannot be rejected. This shows that only the means difference between Case 3.2 and Case 1.1 is statistically significant.

For practical applications, the importance of this difference depends on the desired accuracy of the VFM system. As before, we evaluate the practical significance as a fraction of the mean estimate. In this particular case, the temperature drop of 5 ^{0}C causes the mean estimate error 260.3 bbl/day which is 1.7% relative to the mean value. This is a relatively high value and for many practical cases the consequences of such an error can be critical. Since the VFM might have other factors which cause errors (e.g. noise and drift in pressure sensors), the absence of the correct temperature value can play a crucial role. Overall, we conclude that if the actual fluid temperature changes and the VFM system does not capture this change, it can result in relatively high errors of the flowrate estimations. This fact should be taken into account if there is a probability of the reservoir temperature change in a particular field development case (e.g. water breakthrough).

Heat transfer study

As in the sensor degradation study, we plot the flowrate distributions for the initial visual analysis of the simulation results. **Fig. 18** shows the oil and gas flowrate distributions.

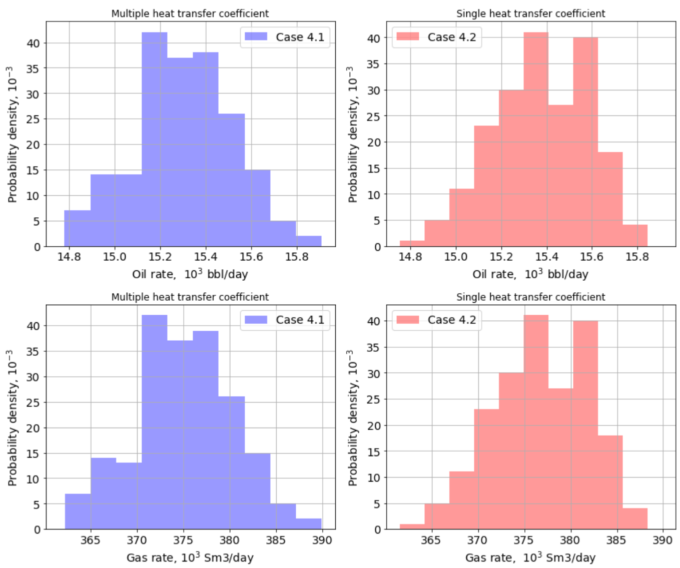

Fig.18 – Histograms of VFM flowrate predictions for Cases 4.x

We see that the flowrate distributions in both cases are relatively similar with some occasional differences in frequency values and may follow the normal distribution pattern. **Fig.19** confirms this observation. As in all the previous cases, except for a few points, the data samples are on the red line which represents the normal distribution. The normality assumption is also supported by D'Agostino test. Even though the flowrate distributions are relatively similar, we quantify the possible differences and evaluate if this difference is practically important for VFM systems.

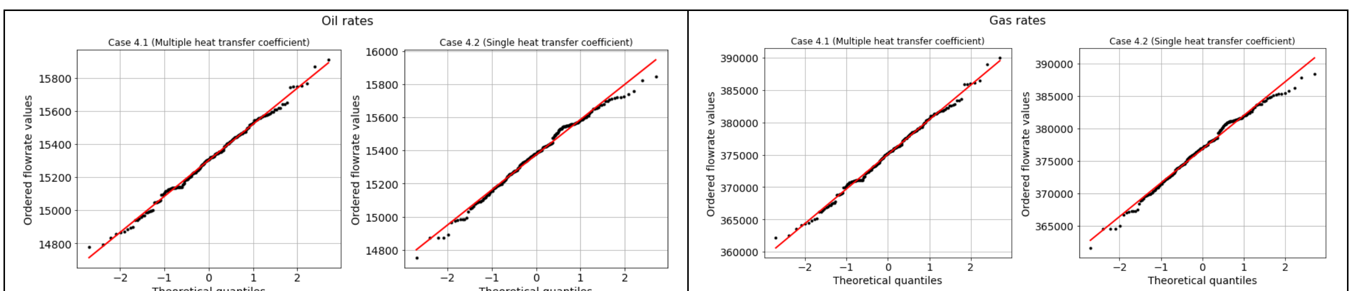

D'Agostino p-value = 0.92	D'Agostino p-value = 0.13	D'Agostino p-value = 0.92	D'Agostino p-value = 0.13

Fig. 19 – Normality testing of datasets from Cases 4.x

Table 7 shows the statistical parameters and hypothesis tests of Case 4.1 and Case 4.2. From the table we see that the difference between the standard deviations is small and can be considered as statistically insignificant. On the other hand, we can reject the hypothesis about the population means equality at the significance level of 0.05. Thus, this difference is considered as statistically significant. However, we can see that this difference is only 0.45% of the mean value and can be considered as practically insignificant. In the sensor degradation case (Case 2), we observed that the increase of the 0.5% drift measurement error introduced approximately 0.5% growth of the error of the mean estimate and we concluded that this difference was practically important. However, in that case we clearly observed the trend between the measurement drift and the estimates. In this case, there error caused by a different tuning strategy most likely will not significantly exceed the error of 0.45% which was computed for this particular case. The deviation may slightly change because of different initial guesses of the heat transfer coefficient values, however, there is not a clear evidence that this difference will increase considerably. Moreover, we observed that the difference of variances even statistically insignificant which also strengthens the point the applied tuning strategies practically give the same result.

	Oil rates	
	Case 4.1	Case 4.2
Mean, bbl/day	15303.34	15373.77
Sample means difference, bbl/day	70.43	
t-test p-value (H_0: $mean_1=mean_2$)	$4.44 \cdot 10^{-5}$	
Standard deviation, bbl/day	216.14	210.96
Standard deviation difference, bbl/day	5.18	
Total range, bbl/day	1131.13	1091.33
Total range difference, bbl/day	39.8	
Bartlett's test p-value (H_0: $var_1 = var_2$)	0.73	
	Gas rates	
	Case 4.1	Case 4.2
Mean, Sm3/day	376917.40	375060.34
Sample mean difference, Sm3/day	1718.79	
t-test p-value (H_0: $mean_1=mean_2$)	$4.47 \cdot 10^{-5}$	
Standard deviation, Sm3/day	5297.55	5172.29
Standard deviation difference, Sm3/day	125.26	
Total range, Sm3/day	27715.52	26752.47
Total range difference, Sm3/day	963.05	
Bartlett's test p-value (H_0: $var_1 = var_2$)	0.74	

Table 7 – Main statistical parameters and hypothesis tests of the simulation results of Cases 4.x

Since we found that the strategies produce very similar results in terms of accuracy, we conclude that the approach with only one tuning heat transfer coefficient is more efficient for practical applications. This is because this approach significantly reduces the computational time for tuning and estimation. In this particular case, the computational time was reduced by a factor of 3. Moreover, computing good initial guesses of the heat transfer coefficients using the physics behind can also take the time. In contrast, initializing a good initial guess of one heat transfer coefficient value is relatively easy and requires only one additional simulation. Therefore, we conclude that the tuning strategy with one heat transfer coefficient along the wellbore is accurate enough and suits better for practical applications than the strategy with multiple heat transfer coefficient values.

Conclusions

In this paper, we constructed a Virtual Flow Meter using a multiphase pipe model and an optimization routine from commercial packages and considered two case studies: the effect of the sensor degradation and two different tuning strategies on the VFM estimates. The sensor degradation effect was modeled as the measurement noise increase, measurement drift and sensors failure. As for the tuning strategies, the use of one versus multiple heat transfer coefficients along the tubing was compared. In addition, we applied a method for a statistical analysis approach of case sensitivity studies which evaluates the distribution of the possible outcomes rather than only critical values for specific boundary conditions.

From the sensor degradation study we found that the noise increase introduces the increase of the flowrate estimates variances and observed close to a linear trend between the noise error and growth of the standard deviation. The quantification of the estimation error growth showed that if the measurement noise becomes relatively large, the associated error should be taken into account. However, if the required VFM accuracy is not high, this error can be neglected in practical applications. On the other hand, the measurement drift can cause more serious estimation deviations since there is almost a linear dependency of the mean estimation value change and the drift measurement error. Thus, it is advisable either to calibrate the sensors (that is hard in practice) or validate the relationship of the VFM predictions and the sensor readings. This can be done by well tests or any other reliable flowrate measurements and preferably carried out more often than a severe sensor drift occurs.

As for the temperature sensor failure, it can be disregarded in case the actual flow temperature does not change. On the other hand, if the actual temperature changes and it is not captured by the VFM, the flowrate predictions can deviate from the correct predictions considerably. This fact should be taken into account if there is a probability of reservoir temperature change.

The case study on different tuning strategies showed that it is not necessary to use a complicated mechanical representation of the well and associated heat transfer coefficients to predict the flowrates accurately. The assumption about the constant heat transfer coefficient along the wellbore gives almost identical results, but can reduce the simulation time substantially. Thus, for practical applications the tuning of a constant heat transfer coefficient along the wellbore is a solid approach.

References

D'Agostino, R. 1971. "An omnibus test of normality for moderate and large size samples." Biometrika 58 (2): 341.

Falcone, G., G. F. Hewitt, and C. Alimonti. 2009. Multiphase Flow Metering: Principles and Applications. Amsterdam: Elsevier.

Falcone, G., G.F. Hewitt, C. Alimonti, and B. Harrison. 2001. "Multiphase Flow Metering: Current Trends and Future Developments." SPR 71474.

Haldipur, P., and G. Metcalf. 2008. "Virtual Metering Technology Field Experience Examples." OTC. Houston, Texas.

Hasan, A.R., and C.S. Kabir. 2012. "Wellbore heat-transfer modeling and applications." Journal of Petroleum Science and Engineering 86-87: 127-136. doi:10.1016/j.petrol.2012.03.021.

Holmås, K., and A. Løvli. 2011. "FlowManager Dynamic: A multiphase flow simulator for online surveillance, optimization and prediction of subsea oil and gas production." 15th International Conference on Multiphase Production . Cannes, France.

Kikani, J., P.S. Fair, and R.H. Hite. 1997. "Pitfalls in Pressure Gauge Performance." SPE Formation Evaluation 12 (04). doi:10.2118/30613-PA.

Lansangan, R. 2012. "A Study on the Impact of Instrument Measurement Uncertainty, Degradation, Availability and Reservoir and Fluid Properties Uncertainty on Calculated Rates of Virtual Metering Systems." 30th International North Sea Flow Measurement Workshop.

Melbø, H., S. Morud, B. Bringedal, R. van der Geest, and K. Stenersen. 2003. "Software That Enables Flow Metering of Well Rates With Long Tiebacks and With Limited or Inaccurate Instrumentation." Offshore Technology Conference.

Patel, P., H. Odden, B. Djoric, R. D. Garner, and H.K. Vea. 2014. "Model Based Multiphase Metering and Production Allocation." Offshore Technology Conference, OTC-25457-MS.

Snedecor, G., and W. Cochran. 1989. Statistical Methods. Iowa State University Press.

Tangen, S., R. Nilsen, and K. Holmås. 2017. "Virtual Flow Meter - Sensitivity Analysis." 35th North Sea Flow Measurement Workshop 2017. Tønsberg, Norway.